

# Human biodistribution and radiation dosimetry of the demyelination tracer [ $^{18}\text{F}$ ]3F4AP

Pedro Brugarolas<sup>#,\*</sup>, Moses Q. Wilks<sup>#</sup>, Jacqueline Noel, Julia-Ann Kaiser, Danielle R. Vesper, Karla M. Ramos-Torres, Nicolas J. Guehl, Marina T. Macdonald-Soccorso, Peter A. Rice, Daniel L. Yokell, Ruth Lim, Marc D. Normandin and Georges El Fakhri<sup>\*</sup>

Gordon Center for Medical Imaging, Department of Radiology, Massachusetts General Hospital and Harvard Medical School, Boston, MA, USA.

<sup>#</sup> Equal contribution

\* Correspondence:

Pedro Brugarolas, Ph.D.  
Gordon Center for Medical Imaging  
Massachusetts General Hospital  
Harvard Medical School  
55 Fruit Street, Bulfinch 051  
Boston, MA 02114  
E-mail: [pbrugarolas@mgh.harvard.edu](mailto:pbrugarolas@mgh.harvard.edu)

Georges El Fakhri, Ph.D., DABR  
Gordon Center for Medical Imaging  
Massachusetts General Hospital  
Harvard Medical School  
125 Nashua Street, Suite 660  
Boston, MA 02114  
E-mail: [elfakhri.georges@mgh.harvard.edu](mailto:elfakhri.georges@mgh.harvard.edu)

1 **Abstract**

2 *Purpose:* [<sup>18</sup>F]3F4AP is a novel PET radiotracer that targets voltage-gated potassium (K<sup>+</sup>) channels and has  
3 shown promise for imaging demyelinated lesions in animal models of neurological diseases. This study  
4 aimed to evaluate the biodistribution, safety and radiation dosimetry of [<sup>18</sup>F]3F4AP in healthy human  
5 volunteers.

6 *Methods:* Four healthy volunteers (2 female) underwent a 4-hour dynamic PET scan from cranial vertex to  
7 mid-thigh using multiple bed positions after administration of  $368 \pm 17.9$  MBq ( $9.94 \pm 0.48$  mCi) of  
8 [<sup>18</sup>F]3F4AP was produced in a cGMP laboratory under IND authorization from the FDA. Volumes of  
9 interest for relevant organs were manually drawn guided by the CT and PET images and time-activity  
10 curves (TACs) were extracted. Radiation dosimetry was estimated from the integrated TACs using  
11 OLINDA software. Safety assessments included measuring vital signs immediately before and after the  
12 scan, monitoring for adverse events, as well as obtaining a comprehensive metabolic panel (CMP) and  
13 electrocardiogram (ECG) within 30 days before and after the scan. The study was approved by the  
14 institutional review board (IRB) and registered at [clinicaltrials.gov](https://clinicaltrials.gov) (NCT04710550) before  
15 commencement.

16 *Results:* [<sup>18</sup>F]3F4AP distributed throughout the body with the highest levels of activity in the kidneys,  
17 urinary bladder, stomach, liver, spleen and brain and with low accumulation in muscle and fat. The tracer  
18 cleared quickly from circulation and from most organs. The clearance of the tracer was noticeably faster  
19 than previously reported clearance in nonhuman primates (NHPs). The average effective dose (ED) across  
20 all subjects was  $12.1 \pm 2.2$   $\mu$ Sv/MBq, which is lower than the estimated ED from the NHP studies ( $21.6 \pm$   
21  $0.6$   $\mu$ Sv/MBq) as well as the ED of other fluorine-18 radiotracers such as [<sup>18</sup>F]FDG ( $\sim 20$   $\mu$ Sv/MBq). No  
22 differences in ED between males and females were observed. No substantial changes in safety assessments  
23 or adverse events were recorded.

24 *Conclusion:* The biodistribution and radiation dosimetry of [<sup>18</sup>F]3F4AP in humans is reported for the first  
25 time. The average total ED across four subjects was lower than most <sup>18</sup>F-labeled PET tracers. The tracer  
26 and study procedures were well tolerated and no adverse events occurred.

27

28

29

30

31 **Keywords:**

32 [<sup>18</sup>F]3F4AP, 4-aminopyridine, PET, biodistribution, radiation dosimetry, IND, first-in-human,  
33 demyelination, multiple sclerosis, voltage-gated potassium channels, fluorine-18.

34

## 1 Background

2 [ $^{18}\text{F}$ ]3-fluoro-4-aminopyridine ([ $^{18}\text{F}$ ]3F4AP) is a radiofluorinated analog of the multiple sclerosis (MS)  
3 drug 4-aminopyridine (dalfampridine, 4AP)[1] (**Fig. 1**). Similar to 4AP, [ $^{18}\text{F}$ ]3F4AP binds to voltage-gated  
4  $\text{K}^+$  channels ( $\text{K}_v1$  family) in demyelinated axons and has been proposed as a PET tracer for imaging  
5 demyelinated lesions in the brain[2-4]. In demyelinated lesions, axonal  $\text{K}^+$  channels  $\text{K}_v1.1$  and  $\text{K}_v1.2$ , which  
6 are normally buried under the myelin sheath and confined to the juxtaparanodal regions of the axons,  
7 become exposed and increase in expression[2-4]. This aberrant expression of  $\text{K}^+$  channels results in  
8 excessive efflux of intracellular  $\text{K}^+$  ions and impaired axonal conduction, thus causing neurological deficits  
9 in MS and other demyelinating diseases. The FDA-approved drug 4AP binds to and blocks the  $\text{K}^+$  channels  
10 in demyelinated axons, reducing the abnormal efflux of  $\text{K}^+$  ions from axons and partially restoring  
11 conduction[5-9]. Given the increase in axonal  $\text{K}^+$  channel expression and the ability of 4AP to bind to these  
12 channels, [ $^{18}\text{F}$ ]3F4AP, a radiofluorinated analog of 4AP, was proposed as a PET tracer for demyelination[1,  
13 10]. [ $^{18}\text{F}$ ]3F4AP is similar to 4AP in that it can enter the brain by passive diffusion and bind to  $\text{K}^+$  channels  
14 in demyelinated axons. Previous studies in rodents showed that [ $^{18}\text{F}$ ]3F4AP can be used to detect lesions in  
15 a rat model of demyelination using PET[1]. Additional studies in rhesus macaques showed that [ $^{18}\text{F}$ ]3F4AP  
16 has suitable properties for imaging primate brains including high brain penetration, fast kinetics, minimal  
17 plasma protein binding and high metabolic stability[11]. Furthermore, PET imaging of a monkey with a  
18 small focal traumatic brain injury sustained three years prior to imaging showed excellent sensitivity to the  
19 lesion[11]. These findings have prompted us to translate [ $^{18}\text{F}$ ]3F4AP to human research studies  
20 (Clinicaltrials.gov identifiers: NCT04699747, NCT04710550). As the first step in the evaluation of  
21 [ $^{18}\text{F}$ ]3F4AP in human subjects, we set out to assess the whole-body biodistribution, safety and radiation  
22 dosimetry in healthy human volunteers. We also compare these results with previous findings in nonhumans  
23 primates.

24



4-aminopyridine  
4AP

[ $^{18}\text{F}$ ]3-fluoro-4-aminopyridine  
[ $^{18}\text{F}$ ]3F4AP

25

26 **Fig. 1.** Chemical structures of 4-aminopyridine and [ $^{18}\text{F}$ ]3-fluoro-4-aminopyridine

27

## 1 **Methods**

2 *Compliance:* the study was approved by the Institutional Review Board at the Massachusetts General  
3 Hospital and registered in [clinicaltrials.gov](https://clinicaltrials.gov) prior to initiation of the study (NCT04710550). [<sup>18</sup>F]3F4AP  
4 was administered under an investigational new drug (IND) authorization from the U.S. Food and Drug  
5 Administration (FDA).

6  
7 *Subjects:* four healthy volunteers (2 females, 2 males) participated in the study after providing informed  
8 consent. Participating criteria included adults between 18 and 65 years old with no history of brain disease  
9 or other serious condition, no contraindications to PET/CT such as severe claustrophobia, accumulated  
10 annual radiation dose less than 30 mSv, not taking dalfampridine containing drugs, normal results on a  
11 complete metabolic panel (CMP) blood test, normal results on electrocardiogram (ECG) and being able to  
12 provide informed consent. No subjects were excluded on the bases of sex, ethnicity or race.

13  
14 *Safety assessments:* vital signs including blood pressure, oxygen saturation and body temperature were  
15 collected immediately before and after completion of the scan. Subjects were queried about their level of  
16 comfort during and after the scan and were told to report any adverse events on the days following the scan.  
17 Within 30 days after completion of the scan, the subjects received a second CMP and a second ECG.

18  
19 *Radiotracer production:* [<sup>18</sup>F]3F4AP synthesis was performed using a Neptis ORA synthesizer as recently  
20 communicated[12]. The synthesis method is based on the previous report by Basuli et al[13]. The tracer  
21 was purified using a semiprep HPLC column (Waters XBridge C18 10 × 250 mm) using 10 mM sodium  
22 phosphate (pH 8) mobile phase containing 5% ethanol. The HPLC fraction containing the product (approx.  
23 10-11 min) was diluted with 10 mL of 0.9% sodium chloride for injection, USP, and passed through a 0.22  
24 μm sterilizing PES filter into a vented 30 mL sterile empty vial. The product vial was visually inspected  
25 and quality control was performed to FDA and USP standards for chemical identity and purity,  
26 radiochemical purity, pH, radionuclidic identity, residual solvents, sterility and bacterial endotoxins. The  
27 sterile filter used was tested for integrity. The dose was released for injection after passing all quality control  
28 tests except for sterility, which was performed after release. All of the batches of [<sup>18</sup>F]3F4AP used in this  
29 study met all product specifications, including sterility test.

30  
31 *Radiotracer administration:* the dose was drawn into a syringe, measured and administered intravenously  
32 as a 1 min infusion through a catheter in the hand or arm. After administration of the dose, the catheter was  
33 flushed with 10 mL of saline and the residual activity in the syringe and catheter measured to calculate the  
34 injected dose.

1 *Image acquisition protocol:* imaging was performed on a GE Discovery MI PET/CT scanner. Subjects were  
2 positioned on the bed of the scanner and a low dose CT from cranial vertex to mid-thigh was acquired.  
3 Based on the CT images, seven bed positions with overlapping edges were selected for PET acquisition (25  
4 cm per bed position with 2.5-5 cm overlap on each end). PET images were acquired over a period of four  
5 hours with two 15 min breaks at approximately 90 min and 160 min after tracer administration. Subjects  
6 were encouraged to void their bladder to eliminate radioactive urine during the breaks. After each break, a  
7 low dose CT was performed for anatomical reference and attenuation correction. The PET acquisition  
8 protocol consisted of a series of static images at each bed position of increasing duration starting upon  
9 administration of the tracer. The full acquisition protocol was as follows: low dose CT, 4 passes  $\times$  1 min  
10 PET acquisition per bed position, 4 passes  $\times$  2 min/bed, break, 2 passes  $\times$  4 min/bed, break, low dose CT,  
11 1 pass  $\times$  7 min/bed position. After completion of the scan, the PET data was reconstructed using the  
12 scanner's VUE Point HD reconstruction algorithm with 17 subsets and 3 iterations with corrections for  
13 scatter, attenuation, deadtime, random coincidence and scanner normalization.

14  
15 *Blood sampling:* 3-5 mL venous blood samples were taken at approximately 8, 30, 60, 90, 135, 165 and  
16 240 min post-injection. Blood samples' radioactivity was counted using a calibrated gamma counter.

17  
18 *Image analysis and dosimetry calculations:* the CT and PET images were coregistered to the first CT  
19 images. Based on the CT and PET images, volumes of interest (VOIs) were manually drawn for the  
20 following tissues: adrenals, brain, breasts, gall bladder, small intestine, upper and lower large intestine,  
21 stomach, heart contents, heart muscle, kidney, liver, lung, muscle, ovaries, pancreas, red marrow, trabecular  
22 and cortical bone, spleen, testes, thymus, thyroid, urinary bladder and uterus. Time-activity curves (TACs)  
23 were extracted for each VOI and uncorrected for decay. TACs were extrapolated to ten half-lives after  
24 injection by assuming that any further decline in radioactivity occurred only due to physical decay with no  
25 biological clearance. Radiation dosimetry and effective dose were calculated from the integrated TACs  
26 using OLINDA software.

## 27 28 **Results**

### 29 *Participant characteristics and radiotracer injection*

30 The demographics of the volunteers are shown in **Table 1**. The study included two males and two  
31 females between the ages of 24 and 59 years old. Three out of the four subjects self-reported to be white  
32 and one reported more than one race. The body mass index of the participants ranged from 21.2 to 33. Each  
33 subject received an intravenous injection of [ $^{18}\text{F}$ ]3F4AP (target activity  $370 \pm 37$  MBq) formulated in ~10  
34 mL of saline (**Table 2**). The molar activity of the tracer at the time of injection was greater than 370

1 GBq/ $\mu$ mol (1 Ci/ $\mu$ mol) as specified on the IND resulting in an injected mass of 3F4AP below 10 microgram,  
2 which is well below the pharmacologically active dose of 4AP (10 mg bid).

3  
4 **Table 1.** Demographics of study participants

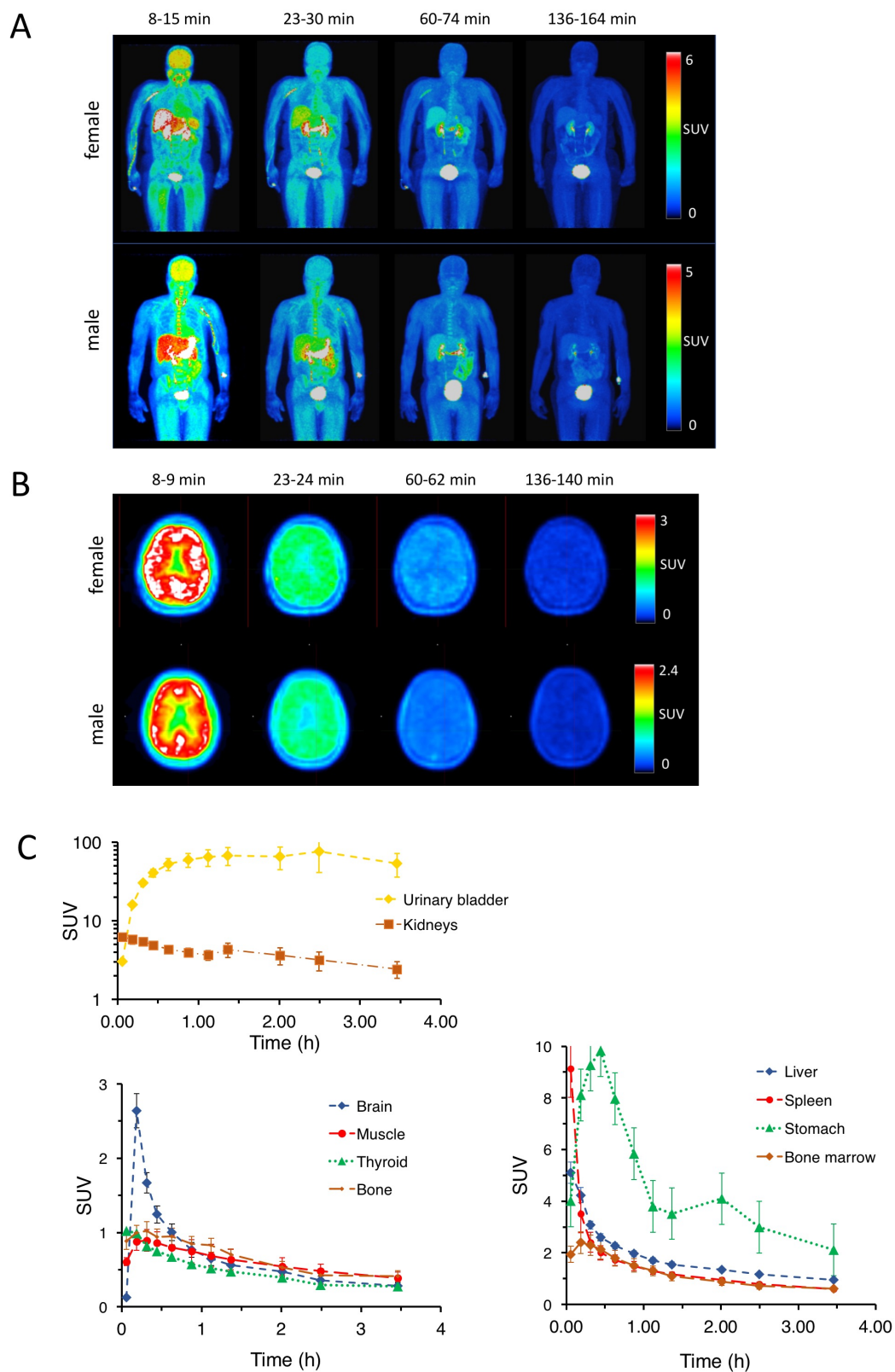
Participant	Sex	Age range (years)	Race/ethnicity	Weight kg (lb)	Height cm (in)	BMI
P1	Female	40-45	Caucasian	79.4 (175)	155 (61)	33
P2	Male	40-45	More than one race	73.5 (162)	175 (69)	24
P3	Male	55-60	Caucasian	61.2 (135)	170 (67)	21.2
P4	Female	20-25	Caucasian	61.2 (135)	163 (64)	23

5  
6 **Table 2.** Injected activity and effective dose for each participant

Participant	Injected Activity MBq (mCi)	Effective Dose mSv
P1	378.14 (10.22)	4.20
P2	381.84 (10.32)	4.89
P3	342.25 (9.25)	3.29
P4	380.73 (10.29)	5.60

7  
8 *Biodistribution and dosimetry*

9 PET imaging started immediately upon tracer administration and consisted of a series of passes  
10 covering the whole body in seven bed positions. To capture the kinetics of the tracer and maximize image  
11 quality, the acquisition time per bed position was short at first (1 min per bed position) and increased over  
12 time (2, 4 and 8 min per bed position). Whole-body and brain PET images at four selected time points are  
13 shown in **Figure 2**. As it can be seen from the images and the accompanying time-activity curves (TACs),  
14 the tracer quickly distributed throughout the whole body including the brain. The maximum activity 8-14  
15 min post-injection can be seen in the liver, kidneys, urinary bladder, spleen, stomach and brain. At 22-28  
16 min post-administration, the highest activity was present in the kidneys, biliary duct and urinary bladder.  
17 After 60 min, most of the activity had cleared from the organs and accumulated in the urinary bladder. Fat  
18 was the tissue type with the lowest activity and no activity accumulation was observed in bone indicative  
19 of no defluorination. The biodistribution seen in the whole-body images indicates rapid clearance primarily  
20 through the kidneys with a small amount of radioactive tracer or metabolites excreted slowly through the  
21 hepatobiliary system.



1  
2 **Fig. 2. [<sup>18</sup>F]3F4AP in human subjects. A.** Representative whole-body maximum intensity projections of a  
3 male and a female participant at different time points. **B.** Representative brain images of a male and a  
4 female participant. **C.** Averaged time-activity curves of selected organs.



1 Organ and whole-body dosimetry were calculated from the TACs using OLINDA software as  
 2 described in the methods. Organs with the highest dose were the heart, urinary bladder and kidneys whereas  
 3 the organs with greater contribution to the effective dose were the ovaries, urinary bladder and testes. The  
 4 calculated average effective dose was  $12.2 \pm 2.2 \mu\text{Sv}/\text{MBq}$  for the four participants and no differences were  
 5 observed between male ( $11.2 \pm 1.6 \mu\text{Sv}/\text{MBq}$ ) and female ( $12.9 \pm 1.8 \mu\text{Sv}/\text{MBq}$ ) participants. The effective  
 6 dose was significantly lower than the effective dose estimated from nonhuman primate studies ( $21.6 \pm 0.6$   
 7  $\mu\text{Sv}/\text{MBq}$ )[11] and the effective dose of other PET tracers ( $[^{18}\text{F}]\text{FDG}$  ED =  $\sim 20 \mu\text{Sv}/\text{MBq}$ [14]). The lower  
 8 ED is likely due to the faster clearance in humans than in nonhuman primates. **Figure 3A** shows averaged  
 9 whole blood radioactivity concentration curves of the four human subjects and two nonhuman primates and  
 10 indicates faster clearance in humans. Interestingly, the blood concentration measured from human blood  
 11 samples is very similar to the concentration in blood obtained from a VOI placed in the left ventricle of the  
 12 heart suggesting that the blood concentration obtained from PET images may provide a good input function  
 13 for pharmacokinetic modeling (**Fig. 3B**).

14

15 **Table 3.** Organ dosimetry calculations. Values are mean  $\pm$  SD of 4 subjects.

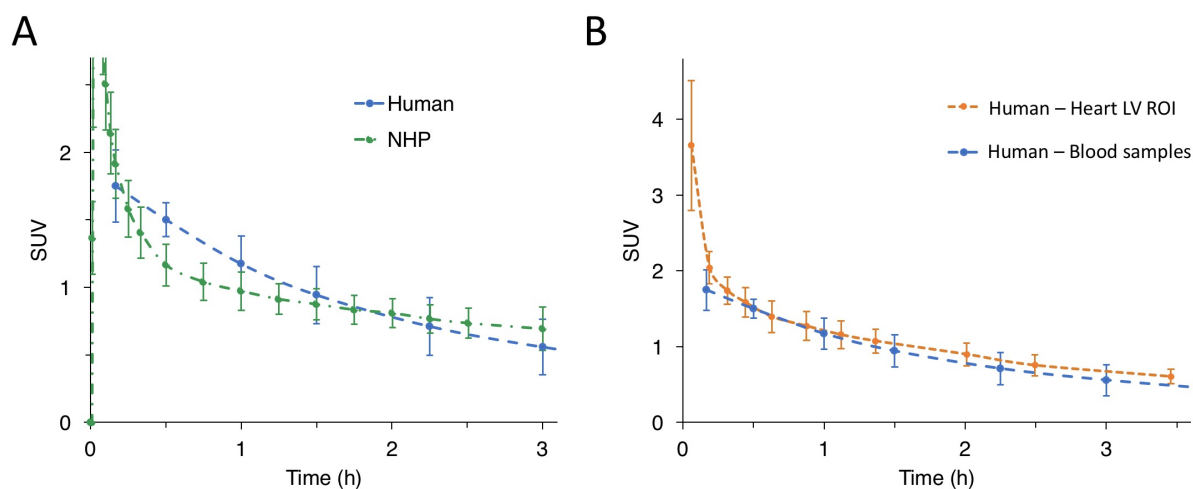
Target Organ	Residence time (h)	Organ Dose ( $\mu\text{Gy}/\text{MBq}$ )	Contribution to ED ( $\mu\text{Sv}/\text{MBq}$ )
Adrenals	$0.0007 \pm 0.0002$	$14.6 \pm 3.6$	$0.073 \pm 0.018$
Brain	$0.031 \pm 0.004$	$6.7 \pm 0.6$	$0.034 \pm 0.003$
Breasts	$0.004 \pm 0.002$	$4.4 \pm 1.1$	$0.221 \pm 0.055$
Gallbladder	$0.0008 \pm 0.0004$	$8.3 \pm 1.0$	0
Lower large intestine	$0.0058 \pm 0.0007$	$8.9 \pm 1.6$	$1.064 \pm 0.196$
Small intestine	$0.017 \pm 0.011$	$8.3 \pm 2.9$	$0.042 \pm 0.015$
Stomach	$0.024 \pm 0.009$	$14.6 \pm 3.6$	$1.750 \pm 0.429$
Upper large intestine	$0.0052 \pm 0.0017$	$7.2 \pm 1.8$	$0.036 \pm 0.009$
Heart	$0.0106 \pm 0.0015$	$54.6 \pm 4.0$	0
Kidneys	$0.039 \pm 0.014$	$28.6 \pm 9.3$	$0.143 \pm 0.046$
Liver	$0.106 \pm 0.018$	$18.4 \pm 1.7$	$0.922 \pm 0.086$
Lungs	$0.015 \pm 0.003$	$8.4 \pm 0.2$	$1.003 \pm 0.027$
Muscle	$0.52 \pm 0.30$	$7.0 \pm 2.3$	$0.035 \pm 0.012$
Ovaries	$0.0007 \pm 0.0005$	$14.9 \pm 4.5$	$2.965 \pm 0.898$
Pancreas	$0.0044 \pm 0.0006$	$15.5 \pm 2.3$	$0.077 \pm 0.011$
Red Marrow	$0.052 \pm 0.020$	$8.6 \pm 2.1$	$1.034 \pm 0.248$
Trabecular bone	$0.015 \pm 0.004$	$13.2 \pm 1.6$	$0.132 \pm 0.016$



Cortical bone	$0.086 \pm 0.024$	$2.6 \pm 0.6$	$0.026 \pm 0.006$
Spleen	$0.009 \pm 0.002$	$15.0 \pm 3.4$	$0.075 \pm 0.017$
Testes	$0.0015 \pm 0.004$	$9.8 \pm 2.2$	$1.950 \pm 0.438$
Thymus	$0.0006 \pm 0.0001$	$11.7 \pm 1.6$	$0.059 \pm 0.008$
Thyroid	$0.0003 \pm 0.0003$	$5.4 \pm 2.2$	$0.271 \pm 0.110$
Urinary bladder	$0.0833 \pm 0.0426$	$51.4 \pm 30.3$	$2.568 \pm 1.512$
Uterus	$0.0015 \pm 0.0015$	$9.4 \pm 6.9$	$0.047 \pm 0.034$

**Total effective dose**  $12.1 \pm 2.2 \mu\text{Sv/MBq}$

1



2

3 **Figure 3. Clearance of  $[^{18}\text{F}]3\text{F4AP}$ .** **A.** Whole blood time-activity curves in human vs. nonhuman primate.  
 4 **B.** Comparison of radioactivity concentration in human blood measured by gamma counting venous  
 5 samples and the concentration derived from an ROI placed in the heart left ventricle in the PET images.  
 6

### 7 *Safety assessment*

8 No significant changes in vital signs (temperature, blood pressure and oxygen saturation) were  
 9 observed before and after the scan. In addition, no significant changes were noted in blood CMP results and  
 10 electrocardiogram results obtained within 30 days before and 30 days after. The tracer and the imaging  
 11 procedure were well tolerated by all the participants and no adverse events occurred during the scan.  
 12

### 13 **Discussion**

14 We present results from the first study with  $[^{18}\text{F}]3\text{F4AP}$  in human research subjects. The goal of  
 15 this study was to assess the biodistribution, radiation dosimetry and safety of  $[^{18}\text{F}]3\text{F4AP}$  in healthy  
 16 volunteers. The study included four healthy adults (two males and two females). The biodistribution and  
 17 calculated effective doses across subjects were found to be very consistent justifying scanning a small  
 18 number of participants. The tracer was found to distribute widely throughout the body including into the

1 brain and clear quickly primarily via renal excretion. The clearance of the tracer was faster than expected  
2 from a previous study in rhesus macaques as evidenced by a faster drop in blood concentration compared  
3 to NHPs. This faster clearance resulted in lower organ doses and a lower effective dose than predicted from  
4 NHP studies. The reasons for the faster clearance may be due to the effects of anesthesia since monkeys  
5 were imaged under anesthesia whereas humans are imaged awake and will be investigated in the future.  
6 Importantly, and as expected, the tracer and study procedures were well tolerated among study participants.

## 7 8 9 **Acknowledgments**

10 The authors thank David Lee, Jr. for providing the fluorine-18 for the radiotracer synthesis. Prof. Brian  
11 Popko from Northwestern University is also acknowledged for supporting the study.

## 12 13 **Author contributions**

14 PB, MQW, NJG, MDN and GEF designed the study. JN, DRV, KMRT, PAR and DLY established the  
15 radiosynthesis method, produced the tracer and performed quality control. JAK, MTMS recruited and  
16 scanned the participants. MTMS and NJG collected the blood samples and analyzed the blood data. RL  
17 supervised the safety aspects of the study. PB, DYL, JAK and GEF prepared the IRB and IND  
18 documentation. PB and MQW analyzed the data and wrote the manuscript, which was reviewed and  
19 approved by all the authors.

## 20 21 **Data availability**

22 The datasets generated during and analyzed during the current study are available from the corresponding  
23 author on reasonable request.

## 24 25 **Funding**

26 This study was partially supported by an Innovation Award from the Polsky Center at the University of  
27 Chicago (PB), NIH R01NS114066 (PB), P41EB022544 (GEF), S10OD026987 (MDN, GEF) and  
28 S10OD018035 (MDN, GEF).

## 29 30 **Competing interest**

31 PB has a financial interest in Fuzionaire Diagnostics and the University of Chicago. PB is a named inventor  
32 of patents related to [<sup>18</sup>F]3F4AP owned by the University of Chicago and licensed to Fuzionaire  
33 Diagnostics. PB's interests were reviewed and are managed by MGH and Mass General Brigham in  
34 accordance with their conflict of interest policies. The other authors declare no conflict of interests.

## References

1. Brugarolas P, Sanchez-Rodriguez JE, Tsai HM, Basuli F, Cheng SH, Zhang X, et al. Development of a PET radioligand for potassium channels to image CNS demyelination. *Sci Rep.* 2018;8:607. doi:10.1038/s41598-017-18747-3.
2. Coman I, Aigrot MS, Seilhean D, Reynolds R, Girault JA, Zalc B, et al. Nodal, paranodal and juxtaparanodal axonal proteins during demyelination and remyelination in multiple sclerosis. *Brain.* 2006;129:3186-95. doi:10.1093/brain/awl144.
3. Arroyo EJ, Sirkowski EE, Chitale R, Scherer SS. Acute demyelination disrupts the molecular organization of peripheral nervous system nodes. *Comp Neurol.* 2004;479:424-34. doi:10.1002/cne.20321.
4. Rasband MN, Trimmer JS, Schwarz TL, Levinson SR, Ellisman MH, Schachner M, et al. Potassium channel distribution, clustering, and function in remyelinating rat axons. *J Neurosci.* 1998;18:36-47.
5. Sherratt RM, Bostock H, Sears TA. Effects of 4-aminopyridine on normal and demyelinated mammalian nerve fibres. *Nature.* 1980;283:570-2.
6. Bostock H, Sears TA, Sherratt RM. The effects of 4-aminopyridine and tetraethylammonium ions on normal and demyelinated mammalian nerve fibres. *J Physiol.* 1981;313:301-15.
7. Jones RE, Heron JR, Foster DH, Snelgar RS, Mason RJ. Effects of 4-aminopyridine in patients with multiple sclerosis. *J Neurol Sci.* 1983;60:353-62.
8. Stefoski D, Davis FA, Faut M, Schauf CL. 4-Aminopyridine improves clinical signs in multiple sclerosis. *Ann Neurol.* 1987;21:71-7. doi:10.1002/ana.410210113.
9. Goodman AD, Brown TR, Krupp LB, Schapiro RT, Schwid SR, Cohen R, et al. Sustained-release oral fampridine in multiple sclerosis: a randomised, double-blind, controlled trial. *Lancet.* 2009;373:732-8. doi:10.1016/S0140-6736(09)60442-6.
10. Brugarolas P, Reich DS, Popko B. Detecting Demyelination by PET: The Lesion as Imaging Target. *Mol Imag.* 2018;17:1536012118785471. doi:10.1177/1536012118785471.
11. Guehl NJ, Ramos-Torres KM, Linnman C, Moon SH, Dhaynaut M, Wilks MQ, et al. Evaluation of the potassium channel tracer [<sup>18</sup>F]3F4AP in rhesus macaques. *J Cereb Blood Flow Metab.* 2021;41:1721-33. doi:10.1177/0271678X20963404.
12. Ramos-Torres K, Noel J, Vesper D, Rice P, Brugarolas P, Yokell D. cGMP production of [<sup>18</sup>F]3F4AP for human PET imaging. *J Nuc Med.* 2021;Suppl. 62, Abstract 1461.
13. Basuli F, Zhang X, Brugarolas P, Reich DS, Swenson RE. An efficient new method for the synthesis of 3-[<sup>18</sup>F]fluoro-4-aminopyridine via Yamada-Curtius rearrangement. *J Labelled Comp Radiopharm.* 2018;61:112-7. doi:10.1002/jlcr.3560.

14. Quinn B, Dauer Z, Pandit-Taskar N, Schoder H, Dauer LT. Radiation dosimetry of  $^{18}\text{F}$ -FDG PET/CT: incorporating exam-specific parameters in dose estimates. *BMC Med Imaging*. 2016;16:41. doi:10.1186/s12880-016-0143-y.